AGU PUBLICATIONS

Space Weather

RESEARCH ARTICLE
10.1002/2015SW001232

Ensemble Modeling of the 23 July 2012 Coronal Mass Ejection

M. D. Cash[1,2], D. A. Biesecker[2], V. Pizzo[2], C. A. de Koning[1,2], G. Millward[1,2], C. N. Arge[3], C. J. Henney[3], and D. Odstrcil[4,5]

[1]Cooperative Institute for Research in Environmental Sciences, University of Colorado Boulder, Boulder, Colorado, USA, [2]Space Weather Prediction Center, National Oceanic and Atmospheric Administration, Boulder, Colorado, USA, [3]Space Vehicles Directorate, Air Force Research Laboratory, Kirtland Air Force Base, New Mexico, USA, [4]School of Physics, Astronomy, and Computational Sciences, George Mason University, Fairfax, Virginia, USA, [5]Heliophysics Science Division, NASA Goddard Space Flight Center, Greenbelt, Maryland, USA

Key Points:
- Quantify effect of model input parameters and SW background on predicted CME arrival time
- Discuss the factors involved in the fast transit time of this large CME
- Present three potential modifications to WSA-Enlil which would enable improved forecasting

Correspondence to:
M. D. Cash,
michele.cash@noaa.gov

Citation:
Cash, M. D., D. A. Biesecker, V. Pizzo, C. A. de Koning, G. Millward, C. N. Arge, C. J. Henney, and D. Odstrcil (2015), Ensemble Modeling of the 23 July 2012 Coronal Mass Ejection, *Space Weather*, *13*, 611–625, doi:10.1002/2015SW001232.

Received 5 JUN 2015
Accepted 29 AUG 2015
Accepted article online 5 SEP 2015
Published online 3 OCT 2015

Abstract On 23 July 2012 a significant and rapid coronal mass ejection (CME) was detected in situ by the Solar Terrestrial Relations Observatory (STEREO) A. This CME was unusual due to its extremely brief Sun-to-1 AU transit time of less than 21 h and its exceptionally high impact speed of 2246 km/s. If this CME had been Earth directed, it would have produced a significant geomagnetic storm with potentially serious consequences. To protect our ground- and space-based assets, there is a clear need to accurately forecast the arrival times of such events using realistic input parameters and models run in near real time. Using Wang-Sheely-Arge (WSA)-Enlil, the operational model currently employed at the NOAA Space Weather Prediction Center, we investigate the sensitivity of the 23 July CME event to model input parameters. Variations in the initial CME speed, angular width, and direction, as well as the ambient solar wind background, are investigated using an ensemble approach to study the effect on the predicted arrival time of the CME at STEREO A. Factors involved in the fast transit time of this large CME are discussed, and potential improvements to modeling such events with the WSA-Enlil model are presented.

1. Introduction

The substantial coronal mass ejection (CME) that erupted from solar active region 11520 (located at ~141°W heliographic longitude) around 0208 UT on 23 July 2012 has generated significant interest within the space weather community for its extremely fast speed and unusual characteristics [e.g., *Russell et al*., 2013; *Baker et al*., 2013; *Liu et al*., 2014; *Ngwira et al*., 2013; *Temmer and Nitta*, 2015]. A detailed discussion of the magnetic field, plasma, and energetic particle aspects of this CME event (as well as a discussion of the timing of events associated with the CME arrival) can be found in *Russell et al*. [2013]. The arrival of a fast forward shock was observed by STEREO A at 2055 UT on 23 July 2012, giving a transit time for the shock front of less than 19 h. Approximately 2 h later, the leading edge of the magnetic cloud was observed at 2255 UT with a peak solar wind speed of 2246 km/s and peak total magnetic field of 109 nT. This CME arrived at 1 AU in near-record time, raising the question: What factors contributed to the exceptional transit time of this CME? And the even more pressing question from a space weather forecasting perspective, if this event had been earthward directed, would we have accurately predicted the arrival time? This paper seeks to address these critical questions.

Using imagery from STEREO A/B [*Kaiser et al*., 2008] and the Solar and Heliospheric Observatory (SOHO) [*Domingo et al*., 1995] as well as in situ data from STEREO A, *Liu et al*. [2014] argue that the fast transit time of the 23 July 2012 CME was caused by preconditioning of the upstream solar wind by an earlier CME that occurred on 19 July. This earlier CME left a low-density region with radial magnetic fields in its wake, which Liu et al. claim resulted in the minimal slowdown of the 23 July event. They also suggest that the in-transit interaction of two closely launched CMEs (both launched early on 23 July approximately 10–15 min apart) resulted in the extreme enhancement of the magnetic structure which impacted STEREO A at 2255 UT on 23 July. Their decision to call this a potential superstorm is based on the solar wind transit speed and the magnetic field. They conclude that the CME-CME interactions in interplanetary space create the potential for a sizeable geomagnetic storm.

Temmer and Nitta [2015] also investigate the propagation behavior of the CME shock and magnetic structure. Using a drag-based model, they aim to reproduce the short transit time and high impact speed observed in situ for this event. They echo the findings of *Liu et al*. [2014] that the minimal deceleration of the CME is

consistent with the preconditioning of the interplanetary space resulting from the passage of a previous CME. They use the drag-based model of *Vršnak et al*. [2013] to reconstruct the CME evolution in the inner heliosphere and find results that strongly indicate that the CME is propagating through a low-density environment. In particular, they find that in order to successfully simulate the CME, the ambient flow speed for the solar wind should be close to the slow solar wind speed (450 km/s) and the density of the ambient solar wind flow must be reduced to 1–2 cm^{-3} at the distance of 1 AU.

At the time of the event, STEREO A was located at 121°W heliographic longitude with a heliocentric distance of 0.96 AU and STEREO B was located at 115°E heliographic longitude with a heliocentric distance of 1.02 AU. While this powerful CME was directed well away from Earth, researchers have speculated as to what might have happened if this event had, in fact, been earthward directed [*Baker et al*., 2013; *Ngwira et al*., 2013]. During this event, the B_z component of the IMF reached a maximum of +87 nT at 2341 UT on 23 July 2012 before turning strongly southward with a minimum B_z of −60 nT occurring at 0057 UT on 24 July 2012. *Baker et al*. [2013] use a geomagnetic storm forecast model [*Temerin and Li*, 2006] to estimate the potential strength of such a storm, and they claim that the 23 July 2012 event could have produced a storm with a storm time disturbance (*Dst*) value ranging from −500 nT to −1182 nT. They argue that the space weather community should use this extreme event to model the potential effect that such a storm could impose on our current technological systems.

In addition to understanding the potential impact that an event similar to the 23 July 2012 CME event could have on Earth, we also need to be able to forecast the arrival time of such a storm at Earth, and that has proven difficult to do for this event. Obtaining the correct CME arrival time using the Wang-Sheely-Arge (WSA)-Enlil solar wind model with realistic input parameters has been challenging, resulting in arrival time predictions late by up to 20 h. In this paper we explore the measurement uncertainties and model limitations contributing to these late-arrival time predictions. Both the CME input parameters and the ambient solar wind background are addressed in this study, and an ensemble of fits is used to quantify the spread in predicted CME arrival times for plausible input parameters. In particular, we explore the sensitivity of the WSA-Enlil solar wind model to a range of possible input parameters, with the specific goal of identifying which input parameters are the most influential in producing the observed rapid transit time of this CME.

An overview of the WSA-Enlil solar wind model and the required model inputs is provided in section 2. In section 3 we discuss how CME input parameters are deduced from geometric analysis of coronagraph images and the large uncertainties associated with fitting this event. In section 4 we explore how variations in the background solar wind influence CME arrival time using different background solar wind maps. We analyze our ensemble to see how variable input parameters influence the expected arrival times (section 5) and to determine if we are able to obtain the correct arrival time when using the WSA-Enlil solar wind model with realistic input parameters. In section 6 we explore the effects of the prior CME on the ambient solar wind, and in section 7 we discuss the results of our ensemble study. Limitations of the WSA-Enlil model and suggested modifications to improve near-real-time (NRT) forecasting for similar future events are discussed in section 8.

2. WSA-Enlil Model

To predict the arrival time of a CME at Earth, we use the coupled Wang-Sheely-Arge (WSA) corona model [*Arge and Pizzo*, 2000; *Arge et al*., 2003, 2004] with the physics-based three-dimensional magnetohydrodynamics (MHD) Enlil solar wind model [*Odstrcil*, 2003]. This is the method currently employed by NOAA's Space Weather Prediction Center (SWPC) to forecast the arrival of earthward directed CMEs [*Pizzo et al*., 2011]. The combined WSA-Enlil model is also installed at NASA's Community Coordinated Modeling Center (CCMC) and is executed in real time at the CCMC Space Weather Research Center [*Mays et al*., 2015]. In addition to the real-time applications, the Air Force Research Laboratory (AFRL) has recently been conducting retrospective studies investigating ensemble forecasting of CMEs using the WSA-Enlil model [*Lee et al*., 2013; *Emmons et al*., 2013].

The WSA model of the solar corona is a combined empirical- and physics-based model of the corona and solar wind that has been adapted from the original Wang and Sheeley model [*Wang and Sheeley*, 1992]. The WSA model uses line-of-sight observations of the photospheric magnetic field as its input. These data are input as full-surface synoptic maps of the photospheric magnetic flux density. The WSA model uses a

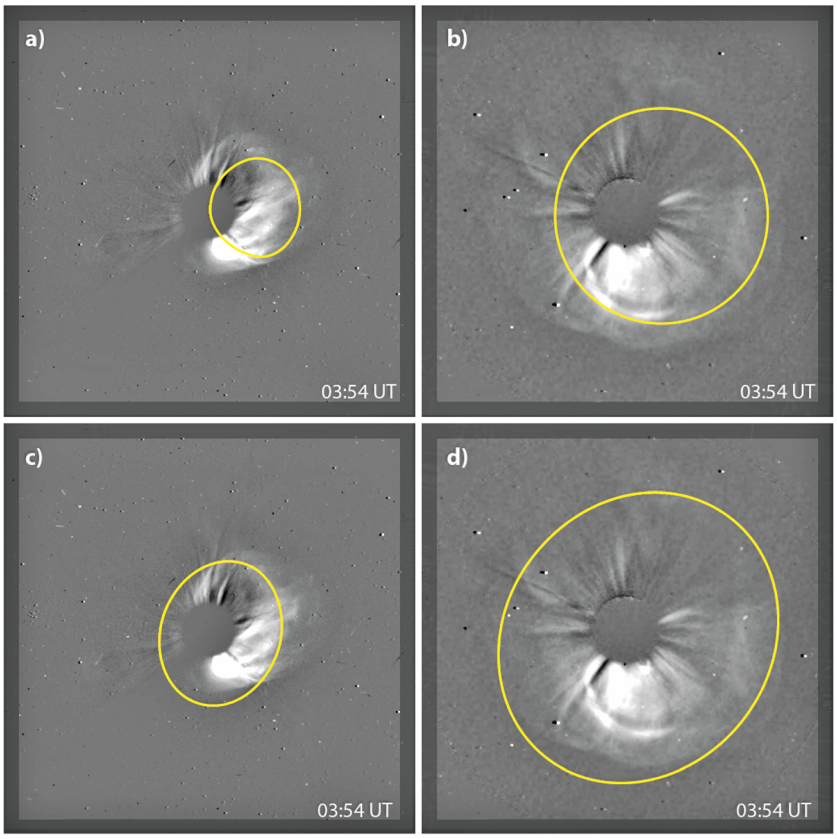

Figure 1. Two different fits of the CME using concurrent images taken by two independent spacecraft. (a, c) SOHO LASCO C3 images of the side of the CME. (b, d) STEREO A COR2 images showing a halo view of the CME. (a, b) A fit using our best estimate of the CME parameters; (c, d) An unreasonably large fit that fails to accurately fit the coronagraph imagery.

magnetostatic potential field source surface model [*Altschuler and Newkirk*, 1969; *Wang and Sheeley*, 1992] to determine the coronal field out to 2.5 solar radii (R_s), which is subsequently extended out to 21.5 R_s using the Schatten Current Sheet model [*Schatten et al*., 1969] to provide the magnetic field of the outer corona. The solution from the WSA model is then used to drive the Enlil solar wind model.

The 3-D MHD Enlil solar wind model developed by *Odstrcil* [2003] simulates the solar wind flow by calculating the solar wind velocity, density, temperature, magnetic field strength, and polarity throughout the inner heliosphere. The model can take into account the preexisting structured ambient solar wind and accurately tracks interactions among multiple ambient and transient structures over a huge spatial domain. To simulate a CME within Enlil, a spherical, hydrodynamic, overpressured pulse is injected at the inner boundary of the numerical model. The parameters required to characterize the CME ejecta include the angular width, speed, direction, and the time at which the CME crosses the inner boundary of the simulation, which is located at 21.5 R_s.

3. Determining CME Parameters

When modeling any CME event, the parameters characterizing the CME ejecta are typically determined via geometric analysis of coronagraph images. The method used by NOAA's Space Weather Prediction Center is a "three-view" technique developed and described by *Millward et al*. [2013], in which a 3-D graphics-based analysis system referred to as the CME Analysis Tool is used to analyze coronagraph images taken concurrently by SOHO and by STEREO A/B. This method involves fitting a 3-D geometric representation of the CME with a lemniscate shape which, compared to the simpler cone shape, more accurately reproduces the curved leading edge of the CME ejecta while still being described in terms of a cone angle and radial size. Once the CME fit parameters have been determined using concurrent images from multiple viewing

Table 1. Summary of CME Fit Parameters for 23 July 2012 CME

			CME Fit Parameters			
	Fitting Method	Conditions[a]	Speed[b]	Longitude	Latitude	Angular Half Width
		This Study				
Fit #1 (Best estimate)	CME analysis tool	NRT Fit	2337 km/s	134.7°	0°	45°
Fit #2	CME analysis tool	NRT Fit	1453 km/s	127.2°	−3.3°	48°
Fit #3	CME analysis tool	NRT Fit	2135 km/s	129.1°	−0.7°	45°
Fit #4	CME analysis tool	NRT Fit	2985 km/s	127.8°	0°	42.5°
Fit #5	CME analysis tool	NRT Fit	1777 km/s	124°	6.7°	53°
Fit parameter variability	CME analysis tool	Mean ± SD	2100 ± 500 km/s	128° ± 4°	0.5° ±3°	47° ± 4°
		Previous Fits				
Baker et al. [2013]	Cone	NRT Fit	3433 km/s	144°	−15°	80°
Baker et al. [2013]	Cone	Post Event	2500 ± 500 km/s	125° + 15° − 5°	2° ± 10°	70° ±15°
Liu et al. [2014]	Triangulation technique of time elongation maps	Post Event	3050 ± 200 km/s	-	-	-
Temmer and Nitta [2015]	Cylindrical shell model	Post Event	2270 ± 420 km/s	125°–135°	0°–10°	65° ± 3° (face-on) 30° ± 3° (edge-on)

[a]NRT fits only use STEREO A and SOHO data while the Post Event fits use all available data.
[b]Average transit speed of 2125 km/s computed by *Russell et al.* [2013].

locations, the CME width and direction parameters are held constant and applied to a time series of images. The CME speed can then be obtained by tracking the leading edge of the CME ejecta in coronagraph images at different times.

For the 23 July 2012 event, there are no real-time STEREO B COR2 [*Howard et al.*, 2008] beacon images from before the launch of the CME at 0208 UT on 23 July 2012, until 0724 UT, which is after the leading edge of the CME has expanded beyond the field of view of the coronagraph. While STEREO B science images are available during the investigated time period, for this study we are interested in our ability to accurately forecast such an event given the available real-time data, and thus we are limited to only using two views to constrain the CME fit. In addition to limited imagery, there is only a handful of times when real-time imagery from the two spacecraft is concurrent (0354 UT, 0454 UT, and 0554 UT).

An example of fitting data for this event using concurrent images from STEREO A and SOHO is shown in Figure 1. On the left side of Figure 1 are images of the side of the CME as viewed by the Large Angle and Spectrometric Coronagraph (LASCO) experiment [*Brueckner et al.*, 1995] instrument on SOHO, and on the right side of Figure 1 STEREO A COR2 head-on images of the CME are shown. Figures 1a and 1b show a fit using our best estimate of the CME parameters, while Figures 1c and 1d show a previously published NRT fit of the CME from *Baker et al.* [2013] that is large in spatial extent and does not represent the data well. The NRT WSA-Enlil model results shown in *Baker et al.* [2013] are initiated at the model inner boundary at 0330 UT on 23 July 2012 with a CME speed of 3435 km/s longitude of 144°, latitude of −15° and half width of 80°. These values are all at the upper end or exceed the upper end of the range determined using coronagraph images, and in our opinion these input parameters are unreasonably large and result in the CME filling the entire sector from ~80°W to beyond 180°W longitude. The average SWPC width for CMEs is 39° with a current upper limit of 60°, and a study by *Burkepile et al.* [2004], which excluded all halo CMEs, found an average CME half width of 26° for 111 limb events with no CMEs having a half width greater than 55°.

Given the real-time limitations of concurrent imagery from only two viewing angles, there is a significant amount of uncertainty in the fit of the CME. Variable CME input parameters for the WSA-Enlil solar wind model include the CME latitude, longitude, half angle, radial velocity, and mass, and a unique solution for these parameters cannot be determined from coronagraph images alone for the 23 July 2012 CME event. For this study, five different fits were made by two individuals based on the available coronagraph imagery. These five fits had CME latitudes ranging from −3.3° to 6.7°, longitudes from 124° to 134.7° (both in Heliocentric Earth Equatorial coordinates), CME half widths from 42.5° to 53° and radial velocities ranging from 1452 km/s to 2985 km/s, representing what we consider to be the extremes of plausible CME fits. Parameters obtained from these five fits are listed in Table 1 along with the mean and standard deviation for all five fits included in this study. Figure 2 illustrates the variability in each of these fits at two different times: the left side shows the fit at 0324 UT and the right side shows the fit half an hour later at 0354 UT.

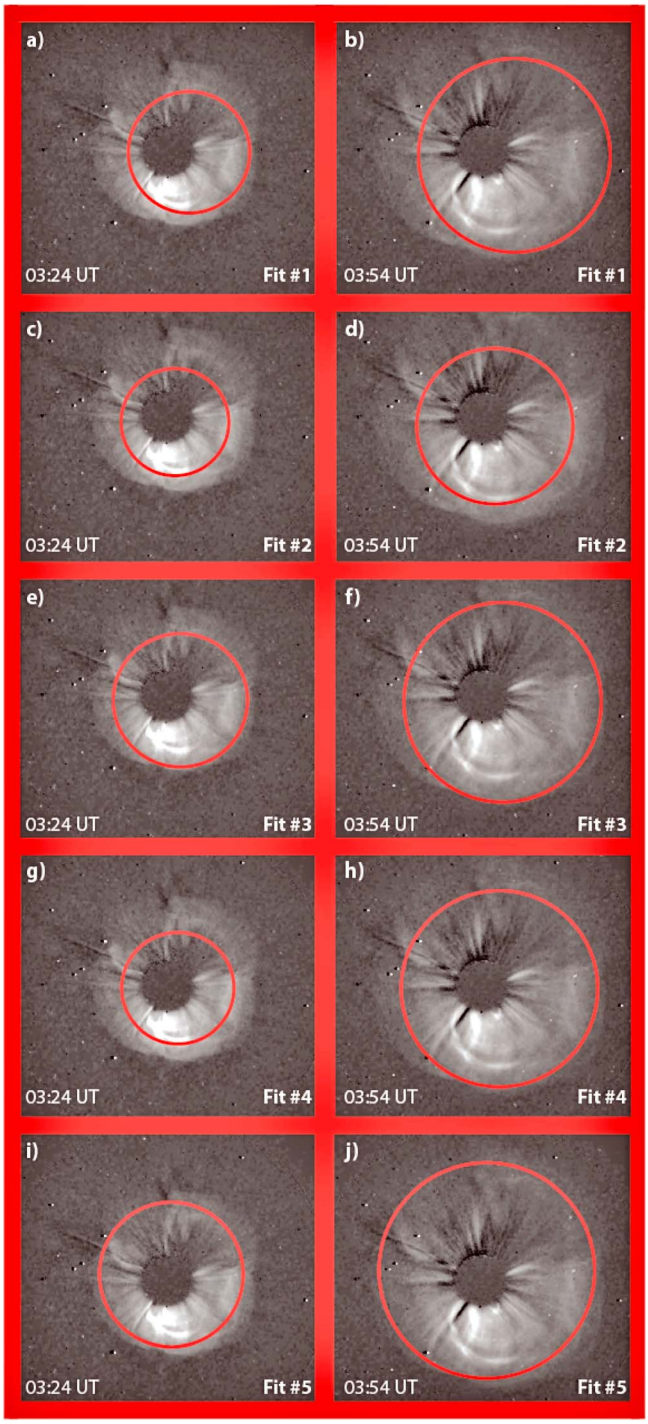

Figure 2. STEREO A COR2 images of the 23 July 2012 halo CME showing five different CME fits. (a, b) This is what we consider to be the best fit for this event. (c, d) A conservative fit in which only obvious CME ejecta material is included. (e, f) A wider fit in which some possible sheath material has been included within the fit in addition to the CME ejecta. (g, h) An inconsistent fit of the CME ejecta where Figure 2g was fit only using the CME ejecta and where Figure 2h includes the CME ejecta as well as the sheath. (i, j) A similar fit to fit one using a wider angular width. Parameters for each fit are listed in Table 1.

Figures 2a and 2b show what we consider to be the best fit for this event (Fit 1). In an ideal fit only the CME ejecta, or driver, is included in the fit and not the usually much wider shock—however, in practice, this can be quite difficult to do. The second CME fit, shown in Figures 2c and 2d, is a conservative fit in which only obvious CME ejecta material is included in the fit. This results in the slowest CME velocity, 1452 km/s. The next fit, Figures 2e and 2f, shows a wider fit in which some possible sheath material has been included within the fit in addition to the CME ejecta. When there is ambiguity as to whether an observed feature is part of the CME ejecta, the SWPC protocol is to include it within the fit. Fit 4 (Figures 2g and 2h) demonstrates an inconsistent fit in which at 0324 UT only the CME ejecta is fit, while at 0354 UT both the CME ejecta and the sheath material are included in the fit. Ideally, the same features ought to be consistently fit in order to get an accurate estimate of the CME velocity. In such an inconsistent fit, the derived CME speed will not accurately represent the true speed of the CME. The final fit (Figures 2i and 2j) is similar to Fit 1 in the features that are fit; however, for this fit a wider angular width was used resulting in a slower-derived CME speed (based on the observed plane of sky speed). Given the difficulty in fitting this CME with the limited imagery available, we consider all five fits in our ensemble in order to cover a range of possible CME fits.

Previous fits of the 23 July 2012 CME published in the literature are summarized in the bottom half of Table 1. It is worth noting that beside the *Baker et al.* [2013] NRT fit and each of our fits, which are based on available NRT coronagraph imagery and use only STEREO A and SOHO data to constrain the fit, all the other published fits include STEREO B data and are post event analyses While the CME fits classified as NRT were

performed using data which were available to space weather forecasters in real time, it is important to recognize that when an analysis is performed post event, it is possible that knowledge from nonreal-time data could influence the result. As indicated in Table 1, *Baker et al*. [2013] include fit parameters for both an NRT fit as well as a post event analysis, in which the CME was determined to have a three-dimensional speed of 2500 ± 500 km/s, a longitude of 125° + 15° − 5°, a latitude of 2° ± 10°, and a half width of 70° ± 15°. The range of these values agrees well with the spread of our chosen values except for the angular width, for which their chosen angular half widths range from 55° to 85°, much larger than the upper end of the range considered in this study of 53°. The face-on angular width determined by *Temmer and Nitta* [2015] using the graduated cylindrical shell model is also larger than the range of half widths determined here, and it is important to consider that different assumptions about CME morphology will often yield different results.

In addition to these five CME fits, we also examine the mass of the CME. In Enlil, the CME mass is computed for the default spherical CME case by considering the mass flux flowing through a spherical cap of varying angular width. The total mass (CME mass + the entrained ambient solar wind mass) is

$$M_{\text{Total}} = 2\pi r_0^3 \rho \left[\omega_{1/2} - \left(\frac{1 - \omega_{1/2}^2}{2} \right) \log \left| \frac{1 - \omega_{1/2}}{1 + \omega_{1/2}} \right| \right], \quad (1)$$

where r_0 is the inner boundary of the simulation (set to 21.5 R_s), $\omega_{1/2}$ is the CME half width (determined from fitting CME), and ρ is the mass density. The product of two reference parameters, dcld and dfast, defines the number density in Enlil, and this is multiplied by the proton mass in order to obtain the mass density. The parameter dcld describes the total injected mass (CME mass plus the entrained ambient solar wind mass) and is typically set to a value of 4. The parameter dfast defines a reference fast stream density and is set to 150 cm^{-3}.

Based on STEREO A and B science data and using the standard method described in *Colaninno and Vourlidas* [2009], we determine a minimum CME mass for this event ranging from 1.4 to 2.1×10^{16}, which is in agreement with the CME mass determined by *Temmer and Nitta* [2015] of $1.5 \pm 0.5 \times 10^{16}$ g. Using the default dcld value of 4 results in CME mass values ranging from 4.9×10^{15} g to 1.1×10^{16} g depending on the CME half width. This default setting, which works for most typical CMEs, appears insufficient for this extreme event. Thus, for this study, dcld was varied from the standard value of 4 to a value of 40.

4. Ambient Solar Wind Background

In addition to variability in the CME input parameters, variations in the ambient solar wind background can significantly influence the transit time of a CME. In this study, daily updated synoptic maps from the National Solar Observatory (NSO) Global Oscillation Network Group (GONG) [*Harvey et al*., 1996] as well as data-assimilated synoptic maps produced by the Air Force Data Assimilative Photospheric flux Transport (ADAPT) model [*Arge et al*., 2010, 2011; *Henney et al*., 2012; *Hickmann et al*., 2015] are used as input into the WSA model. Currently, NOAA/SWPC uses the GONG 2 h updated synoptic maps to drive the WSA model. However, work by *Lee et al*. [2013] suggests that better results can be obtained using the data-assimilated synoptic maps produced by ADAPT, which provide a potentially more realistic snapshot of the global photospheric magnetic field by incorporating magnetic flux transport within the model calculations.

To determine how variations in the ambient solar wind background influence the transit time of the 23 July 2012 CME, we consider three different solar wind background maps in this ensemble study: a GONG map from 23 July 2012 and two ADAPT maps, one from 25 July 2012 and one from 26 July 2012. The later ADAPT maps, while incorporating data from after the arrival of the CME on 23 July, allow us to test how much improvement in the model result we could expect given a more realistic ambient solar wind background. The maps from 25 and 26 July incorporate previously out-of-view far side active regions, whose inclusion provide a much more realistic global representation of the photospheric magnetic field distribution and hence improved predictions of both the corona and ambient solar wind.

Differences between these three solar wind backgrounds can be observed in Figure 3, which shows the plasma density (top) and radial velocity (bottom) for the three background maps used in this study. These runs all use the same CME parameters, Fit 1 in Table 1 with a CME mass of 6.0×10^{15} g and show the CME

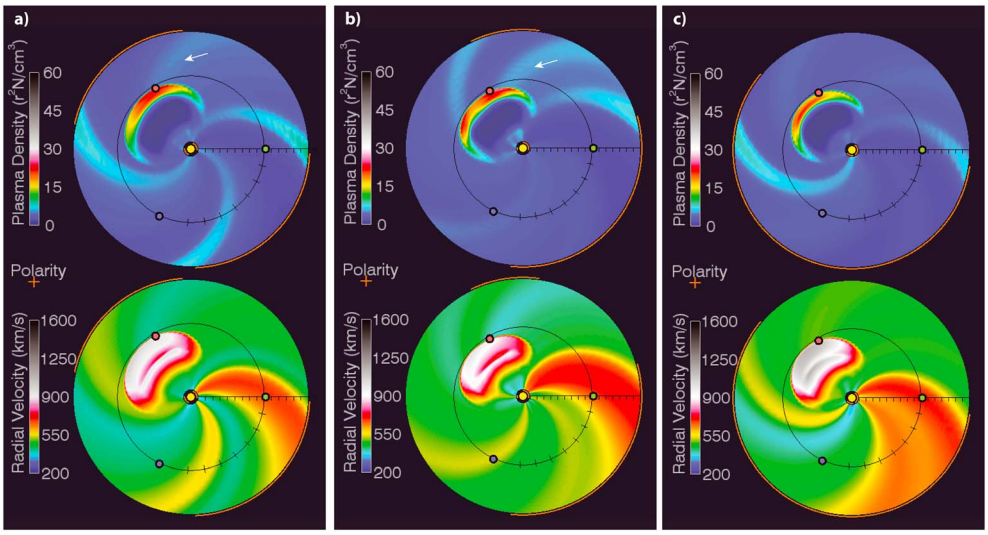

Figure 3. Results from WSA-Enlil solar wind model using three different solar wind background maps but with the same CME parameters (Fit 1 with a mass of 6.0×10^{15} g). (a) GONG-generated solar wind background from 23 July 2012. (b) ADAPT map for 25 July 2012. (c) ADAPT map for 26 July 2012. In this equatorial view, the yellow circle represents the Sun, the green circle is the Earth, the red circle shows the location of STEREO A, and the blue circle marks the location of STEREO B. Note the absence in Figure 3c of the stream interface, indicated by the white arrows, which is preceding the CME in Figures 3a and 3b.

at the time that it reaches STEREO A (see Table 2, runs 1–3 for input parameters and arrival time information). In the GONG-generated background (Figure 3a) and the ADAPT map from 25 July (Figure 3b), a stream interaction region is observed ahead of the CME and is indicated by a white arrow in the image. In the ADAPT map from 26 July (Figure 3c), this stream interface is not present. These subtle differences in the background solar wind can influence the predicted arrival times as discussed in section 5, and we expect to obtain the most accurate arrival time predictions using background solar wind maps that most closely match the data.

To determine which maps most closely resemble the data, we compare output obtained using only WSA, without Enlil, to in situ data from the Advanced Composition Explorer (ACE) and STEREO A spacecrafts. Figure 4 shows WSA velocity predictions at both the location of ACE and STEREO A for ADAPT maps initialized using magnetograms from three different days. Predictions for the solar wind at ACE are shown on the left side (Figures 4a–4c) and on the right are predictions for the solar wind at STEREO A (Figures 4d–4f). Figures 4a and 4d show ADAPT maps for 22 July, Figures 4b and 4e show ADAPT maps for 25 July, and Figures 4c and 4f for 26 July. Looking at the solar wind results (observed versus WSA predicted) for an ADAPT photospheric field map from 22 July (Figure 4a), the solar wind speed predictions agree poorly with observations.

Using an ADAPT map from 4 days later (25 July, Figure 4b), however, we find that the fit is much improved, except for the 21–24 July period. Due to the presence of several CMEs during 21–24 July, getting the correct solar wind for the 21–24 July period is not expected. Using ADAPT maps from 25 and 26 July give better global solar wind results for STEREO A and ACE for the time period of interest. By 25 July, the majority of the new activity that emerged on the far side of the Sun has rotated onto the frontside and been assimilated into the model. STEREO A results are best for 26 July 2012 because, by this time, a new active region has finished emerging on the frontside of the Sun. As can be seen in these plots, a few days difference in time can produce a significant change in WSA results.

Another way to identify which solar wind maps most closely resemble the background through which the CME propagated out is to determine whether the stream structure observed in the GONG map and 25 July ADAPT map (Figures 3a and 3b) is actually present in the solar wind data. One way to do this is to look for solar sector crossings observed by ACE and STEREO A/B in the rotations before and after the 23 July 2012 event. In the solar wind data from 17 June 2012 through 28 August 2012, there is no strong evidence for a persistent stream interface observed ahead of the 23 July CME. Source surface synoptic charts provided by

Space Weather

10.1002/2015SW001232

Table 2. Table of All Ensemble CME Parameters[a]

	CME Input Parameters									
Run #	CME Fit #	CME Axis Lat. (deg)	CME Axis Lon. (deg)	Half-Width Angle (deg)	Radial Velocity (km/s)	dcld	CME Mass (g)	SW Background	Expected Arrival Time at 1 AU[b]	Prediction Error (h)
1	1	0	134.7	45	2337	4	5.99E+15	GONG	7/24/2012 06:00	9.0
2	1	0	134.7	45	2337	4	5.99E+15	ADAPT 25th	7/24/2012 07:00	10.0
3	1	0	134.7	45	2337	4	5.99E+15	ADAPT 26th	7/24/2012 04:00	7.0
4	1	0	134.7	45	2337	8	1.40E+16	GONG	7/24/2012 02:00	5.0
5	1	0	134.7	45	2337	8	1.40E+16	ADAPT 25th	7/24/2012 02:00	5.0
6	1	0	134.7	45	2337	8	1.40E+16	ADAPT 26th	7/24/2012 00:30	3.5
7	**1**	**0**	**134.7**	**45**	**2337**	**40**	**7.79E+16**	**GONG**	**7/23/2012 21:30**	**0.5**
8	**1**	**0**	**134.7**	**45**	**2337**	**40**	**7.79E+16**	**ADAPT 25th**	**7/23/2012 21:00**	**0.0**
9	**1**	**0**	**134.7**	**45**	**2337**	**40**	**7.79E+16**	**ADAPT 26th**	**7/23/2012 21:00**	**0.0**
10	2	−3.3	127.2	48	1453	4	7.56E+15	GONG	7/24/2012 15:00	18.0
11	2	−3.3	127.2	48	1453	4	7.56E+15	ADAPT 25th	7/24/2012 16:30	19.5
12	2	−3.3	127.2	48	1453	4	7.56E+15	ADAPT 26th	7/24/2012 13:30	16.5
13	3	−0.7	129.1	45	2135	4	6.07E+15	GONG	7/24/2012 07:30	10.5
14	3	−0.7	129.1	45	2135	4	6.07E+15	ADAPT 25th	7/24/2012 08:30	11.5
15	3	−0.7	129.1	45	2135	4	6.07E+15	ADAPT 26th	7/24/2012 05:30	8.5
16	3	−0.7	129.1	45	2135	15	2.83E+16	GONG	7/24/2012 00:30	3.5
17	3	−0.7	129.1	45	2135	15	2.83E+16	ADAPT 25th	7/24/2012 01:00	4.0
18	3	−0.7	129.1	45	2135	15	2.83E+16	ADAPT 26th	7/24/2012 00:00	3.0
19	4	0	127.8	42.5	2985	4	4.93E+15	GONG	7/24/2012 02:00	5.0
20	4	0	127.8	42.5	2985	4	4.93E+15	ADAPT 25th	7/24/2012 03:00	6.0
21	4	0	127.8	42.5	2985	4	4.93E+15	ADAPT 26th	7/24/2012 00:30	3.5
22	**4**	**0**	**127.8**	**42.5**	**2985**	**8**	**1.15E+16**	**GONG**	**7/23/2012 22:00**	**1.0**
23	4	0	127.8	42.5	2985	8	1.15E+16	ADAPT 25th	7/23/2012 22:30	1.5
24	**4**	**0**	**127.8**	**42.5**	**2985**	**8**	**1.15E + 16**	**ADAPT 26th**	**7/23/2012 21:00**	**0.0**
25	4	0	127.8	42.5	2985	20	3.12E+16	GONG	7/23/2012 18:30	−2.5
26	4	0	127.8	42.5	2985	20	3.12E+16	ADAPT 25th	7/23/2012 18:30	−2.5
27	4	0	127.8	42.5	2985	20	3.12E+16	ADAPT 26th	7/23/2012 18:30	−2.5
28	4	0	127.8	42.5	2985	40	6.41E+16	GONG	7/23/2012 17:30	−3.5
29	4	0	127.8	42.5	2985	40	6.41E+16	ADAPT 25th	7/23/2012 17:30	−3.5
30	4	0	127.8	42.5	2985	40	6.41E+16	ADAPT 26th	7/23/2012 17:30	−3.5
31	5	6.7	124	53	1777	4	1.11E+16	GONG	7/24/2012 10:00	13.0
32	5	6.7	124	53	1777	4	1.11E+16	ADAPT 25th	7/24/2012 11:30	14.5
33	5	6.7	124	53	1777	4	1.11E+16	ADAPT 26th	7/24/2012 08:30	11.5
34	1	0	134.7	45	2337	4	5.99E+15	Dens. = 3.6 cm^{-3}	7/24/2012 03:00	6.0

Table 2. (continued)

	CME Input Parameters									
Run #	CME Fit #	CME Axis Lat. (deg)	CME Axis Lon. (deg)	Half-Width Angle (deg)	Radial Velocity (km/s)	dcld	CME Mass (g)	SW Background	Expected Arrival Time at 1 AU[b]	Prediction Error (h)
35	1	0	134.7	45	2337	4	2.00E+15	Density = 1.2 cm^{-3}	7/23/2012 22:30	1.5
36	1	0	134.7	45	2337	8	1.40E+16	Density = 3.6 cm^{-3}	7/24/2012 00:00	3.0
37	**1**	**0**	**134.7**	**45**	**2337**	**8**	**4.66E+15**	**Density = 1.2 cm^{-3}**	**7/23/2012 21:00**	**0.0**
38	**1**	**0**	**134.7**	**45**	**2337**	**20**	**3.79E+16**	**Density = 3.6 cm^{-3}**	**7/23/2012 21:30**	**0.5**
39	**1**	**0**	**134.7**	**45**	**2337**	**20**	**1.26E+16**	**Density = 1.2 cm^{-3}**	**7/23/2012 21:00**	**0.0**

[a]Bold text indicates runs in which the predicted CME arrival time was within ± 1 h of the observed CME arrival time.
[b]Dates are formatted as month/day/year.

the Wilcox Solar Observatory for 21 June 2012 through 15 August 2012 also indicate that it is unlikely that a stream interface preceded the 23 July CME. Determining whether a stream interface was in fact present helps us to identify which solar wind background map most closely resembles the actual ambient solar wind during this time period. If a stream structure is present in the background solar wind, then a more massive CME is required to push through the density enhancement associated with the stream interface.

5. Variability in Predicted CME Arrival Times

The various CME fits determined in section 3 combined with the assumed CME mass and the ambient solar wind background maps discussed in section 4 provide an ensemble of model runs from which we can examine the sensitivity of the model results to a range of input parameters. With this ensemble, our main objective is to quantify the extent of variability in the predicted CME arrival time and to determine if, given realistic input parameters, we can obtain a predicted CME arrival time that agrees with the observed arrival time at STEREO A. When comparing arrival times, we focus on the arrival time of the forward shock that passed STEREO A at 2055 UT on 23 July and is evident by a large jump in the solar wind velocity which increased from 900 km/s to over 2200 km/s across the shock [see *Russell et al.*, 2013; *Liu et al.*, 2014]. For each ensemble member, we determined the arrival time based on the predicted jump in the radial velocity and plasma density obtained from the Enlil solar wind model. Results are given in Table 2, which lists the CME input parameters, solar wind background used, predicted arrival time at STEREO A, and the prediction error to the nearest half hour.

Predicted CME arrival times ranged from 23 July 2012 at 1730 UT (using a mass of 6.41×10^{16} g and a velocity of 2985 km/s) to the CME arriving on 24 July 2012 at 1630 UT (using a mass of 7.56×10^{15} g and a velocity of 1452 km/s). This represents a spread of ~24 h in the predicted CME arrival time depending on CME fit parameters, background solar wind, and the assumed mass of the CME. For this event, the parameters that most influenced the CME arrival time included the CME velocity, mass, and half width, while getting the CME axis latitude and longitude right was found to be not as critical (Table 3). The greatest variability in the predicted CME arrival time resulted from the uncertainty in the radial velocity, with a spread of ±7 h in arrival time. The next most influential CME parameters are the CME mass which resulted in a spread in arrival time of ±4.6 h and the CME half width, which is related to the CME mass (see section 2), and resulted in a spread of 4.3 h in the CME arrival time.

Figure 5 illustrates the spread in the modeled arrival time for two different CME fits (Fit 1 and Fit 4, see Table 1 for fit parameters) for a range of CME masses and ambient solar wind backgrounds. The lowest-mass CME runs are shown in blue and green and the most massive CME runs are in red and orange. The ambient solar wind background map that was used is denoted by the line style,

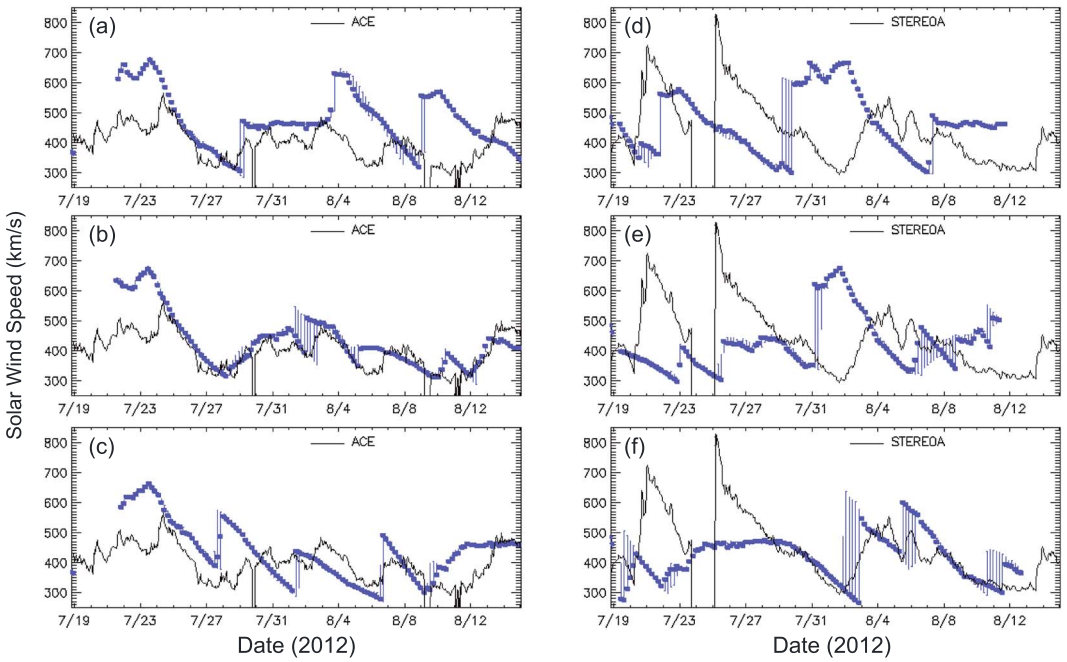

Figure 4. Prediction of solar wind speed at (left) ACE and at (right) STEREO A based on ADAPT maps for (top) 22, (middle) 25, and (bottom) 26 July 2012. The black line represents the solar wind speed measured by the spacecraft and the blue squares show the solar wind speed predicted by the ADAPT maps. The black spikes in Figures 4d–4f result from CMEs and are not included in the ADAPT background solar wind predictions.

with a solid line indicating the use of the GONG background map from 23 July, a dashed line indicating the 25 July ADAPT map, and a dash-dotted line indicating that the 26 July ADAPT map was used. Figure 5 clearly illustrates the arrival time-mass dependence observed for each of the two CME fits shown. The choice of the ambient solar wind background structure is observed to be more critical for less massive CMEs (blue and green lines) than it is for the most massive events (red and orange lines), for which the predicted CME arrival time is independent of the ambient solar wind background. A massive CME can more easily push through background stream structures with the result that background solar wind density structure becomes less influential as the CME mass increases.

In Figure 5, the actual solar wind velocity values observed by the STEREO A PLASTIC instrument are plotted using grey "plus" symbols. Extreme input velocities and masses, such as those depicted by the red and orange lines in Figure 5b, result in a model velocity that is much higher than what was actually observed at STEREO A and a predicted arrival time much too early. However, more reasonable input parameters such as those shown by the green lines in Figure 5a result in a too late arrival time and a predicted CME speed at STEREO A which was lower than that which was actually observed (2246 km/s). This suggests that the CME experienced minimal slowdown during its travel to 1 AU. These results agree with work by *Liu et al.* [2014] and *Temmer and Nitta* [2015], who postulate that a preceding CME, which occurred 4 days earlier on 19 July 2012, left a low-density region with radial magnetic fields in its wake, resulting in the minimal slowdown of the 23 July 2012 CME.

Table 3. Variability in Predicted CME Arrival Time With Varying Input Parameters

Parameter	Variability in Input	Average Variability in Arrival Time
Radial velocity (dcld = 4)	1453 to 2985 km/s	±7.0 h
CME mass (Velocity = 2337 km/s)	5.99E+15 to 7.79E+16 g	±4.6 h
CME half angle	42.5 to 53°	±4.3 h
CME axis latitude	−3.3 to 6.7°	±2.7 h
SW background (Velocity = 2337 km/s)	1.2 to 3.6 cm^{-3} at 1 AU	±2.5 h
CME axis longitude	124 to 134.7°	±2.1 h

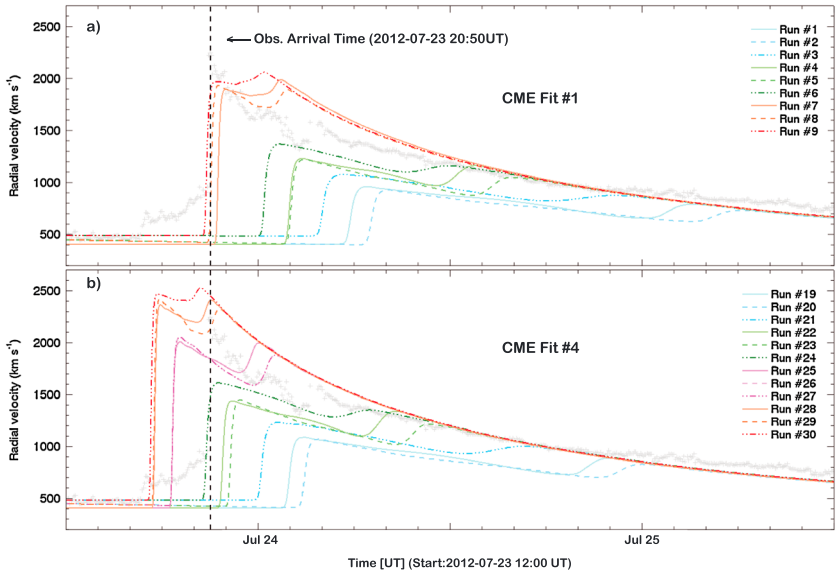

Figure 5. Example model output for two different CME fits for a range of CME masses and ambient solar wind backgrounds. (a) Ensemble results for CME fit 1, runs 1–9 in Table 2. (b) Result for CME fit 4 for runs 19–30 in Table 2. Line color corresponds to the CME mass with the lowest mass CME runs shown in blue and the most massive CME runs shown in red and orange. The ambient solar wind background map used is denoted by the line style, with a solid line indicting the use of the GONG background map from 23 July, a dashed line used for the 25 July ADAPT map, and a dashed and dotted line indicating that the 26 July ADAPT map was used. The choice of the ambient solar wind background is observed to be more critical for less massive CMEs (blue and green lines) than it is for the most massive events (red and orange lines), for which the predicted CME arrival time is independent of the ambient solar wind background. The solar wind velocity observed by STEREO A is denoted by the grey "plus" symbols.

6. Preconditioning of Solar Wind Due To Earlier CME

When modeling the two successive CMEs with WSA-Enlil, each CME is treated independently. As soon as the first CME moves beyond Enlil's inner boundary, the model reverts to using the specified background map and any stream interfaces present reform instantaneously before the launch of the second CME. Therefore, given the current operational version of WSA-Enlil, the preceding CME that was launched on 19 July 2012 at approximately 0530 UT does not influence the predicted arrival time of the subsequent CME 4 days later. However, as discussed in *Liu et al.* [2014] and *Temmer and Nitta* [2015], following in the wake of the earlier 19 July CME was a density depletion region in which the density remained very low until the arrival of the 23 July event, and this preconditioned, low-density solar wind appears to be an important factor in obtaining the correct CME arrival time.

Neither the GONG nor the ADAPT background maps are representative of the solar wind observed at STEREO A before the arrival of the 23 July CME, demonstrating that by limiting ourselves to using standard background maps, we are constrained in the variety of backgrounds included in our ensemble. The GONG and ADAPT synoptic maps, which are based on photospheric magnetic field observations, do not include the potential effects of this earlier CME on the ambient background solar wind, and so to simulate the observed preconditioned solar wind properties with Enlil, we consider a uniform hydrodynamic background representative of the post-CME flow. We examine two different ambient backgrounds with densities at 1 AU of 3.6 cm^{-3} and 1.2 cm^{-3} and each with a constant velocity of 450 km/s [see *Baker et al.*, 2013; *Liu et al.*, 2014]. As mentioned above, the Enlil model rapidly reverts to the ambient background solar wind and any stream interfaces present reform immediately after a CME moves beyond the simulation's inner boundary. Using these uniform solar wind background maps enables us to circumvent this model constraint and to recreate the solar wind conditions observed at STEREO A in the wake of the preceding CME.

Model results using the hydrodynamic backgrounds are listed at the end of Table 2 and are shown in Figure 6. For the background map with a constant density of 3.6 cm^{-3}, the predicted CME arrival times are similar to those obtained using the ADAPT map from 26 July (i.e., CME fit #1 with dcld set to 4 is predicted to arrive

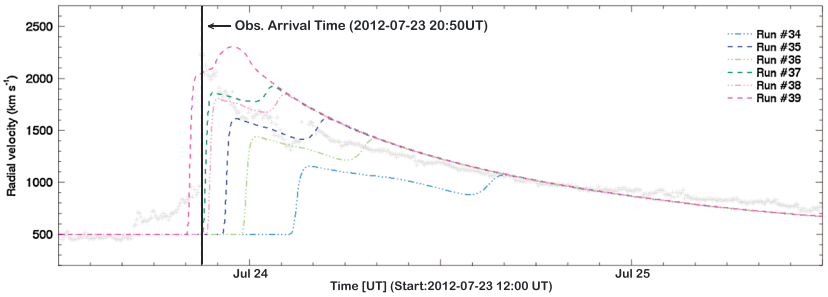

Figure 6. Same format as Figure 5 showing ensemble results for fit 1 in the hydrodynamic background cases, runs 34–39 in Table 2. The dashed line represents the 1.2 cm^{-3} density background and the dashed dotted line represents the 3.6 cm^{-3} density background. The lowest mass CME runs are shown in blue, and the most massive CME runs are in mauve.

on 24 July 2012 at 0300 UT using the hydrodynamic background versus a predicted arrival time on 24 July 2012 at 0400 UT using the ADAPT map from 26 July). However, when the density of the background solar wind is reduced to 1.2 cm^{-3} (dashed lines in Figure 6) and all else is held constant, significantly shorter CME transit times are observed, with the CME traveling through the lower density ambient predicted to arrive 5 h earlier (see Table 2, runs 34–35).

In Enlil, as discussed in section 3, the computed CME mass is directly proportional to the parameter dfast, which defines the reference fast stream density. This same parameter is also used to compute the mass density of the background solar wind, and so by decreasing the background solar wind density by a third (and hence decreasing dfast), the mass of the CME also decreased by an equivalent amount. For the 1.2 cm^{-3} density ambient background, if the mass ratio parameter dcld is increased from 4 to 8 (giving a CME mass of 4.7×10^{15} g), then the CME is predicted to arrive 1.5 h earlier and a CME shock arrival time of 2113 UT on 23 July 2012 is predicted using the Enlil model. If we further increase dcld to 20, then the CME mass increases to 1.3×10^{16} g and is predicted to arrive ~30 min earlier at 2049 UT on 23 July 2012. This CME mass is still less than the minimum CME mass estimates, which range from 1.4 to 2.1×10^{16} g for this event. However, in the slightly denser hydrodynamic background (3.6 cm^{-3}), a dcld value of 20 gives a CME mass of 3.8×10^{16} g and the CME shock's predicted arrival time is 2130 UT on 23 July 2012, which is within 35 min of the observed shock arrival time.

7. Ensemble Results

Using the WSA-Enlil solar wind model, we are able to obtain the observed CME arrival time, to within ±1 h, for 8 of our 39 model runs (Figure 7). These runs, presented in boldface in Table 2, are for two different CME fits and cover the full range of solar wind backgrounds included in this analysis. For the runs using the GONG and

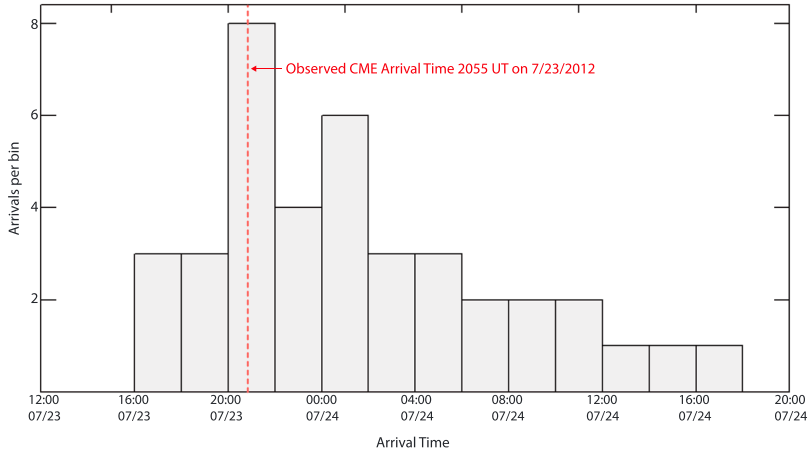

Figure 7. Frequency distribution of CME arrival times for the ensemble study of 39 individual CME fits. The red line indicates the observed CME arrival time at 2055 UT on 23 July 2012.

ADAPT solar wind background maps, when using the first CME fit for which a reasonable CME velocity of 2337 km/s was obtained, an extremely large mass of 7.79×10^{16} g was required in order to predict the correct CME arrival time. By assuming a very massive CME, the predicted arrival time was independent of the solar wind background. As discussed above, the solar wind background influences CME arrival times for very fast, but less massive CMEs.

Using a more conservative mass of 1.15×10^{16} g, the correct arrival time can also be obtained using the ADAPT map from 26 July and a CME speed of 2985 km/s. However, as discussed in section 3, this CME speed is likely an overestimate. For this fast, but less massive case, the solar wind background influences the propagation of the CME through the inner heliosphere and only for the ADAPT background from 26 July is the predicted arrival time in agreement with the observed arrival time. In background maps from 23 July (GONG) and 25 July (ADAPT), the presence of the stream interface seen in Figure 3 slows down the CME, resulting in an arrival time approximately 1 h later at 2200 UT on 23 July 2012. As the CME mass is increased, the arrival time is progressively earlier (see Table 2, runs 25–30). For runs with the fastest CME velocities (2985 km/s) and largest masses ($\geq 3.12 \times 10^{16}$ g), the predicted arrival times are much earlier than the arrival time observed at STEREO A, suggesting an upper limit on the velocity and mass of the 23 July 2012 CME.

Model results using the two hydrodynamic backgrounds discussed in section 6 suggest that there is probably a range of possible combinations of assumed CME mass and background solar wind density and speed that enable a CME with realistic fit parameters to complete the transit to STEREO A in the observed amount of time. We find that using a low-density uniform hydrodynamic background representative of the post-CME flow is an important factor in modeling this event, and these findings are in agreement with the results of *Temmer and Nitta* [2015], which were able to model the arrival time by decreasing the drag for their CME parameters.

This work suggests that if this event had been earthward directed, given the current operational setup at SWPC, we would not have been able to accurately predict the arrival time of this extreme event. In order to obtain the observed arrival time, the CME mass had to be increased in all cases, and the best agreement was obtained when a uniform density hydrodynamic background that closely matched the observed plasma parameters, just upstream of the shock at STEREO A, was employed.

8. Summary and Conclusion

These results suggest that improvements to the operational version of the WSA-Enlil model may be necessary, including modification to the strategy for determining how much mass is input into the WSA-Enlil model, CME configuration, and correcting in near real time the background solar wind when necessary. As has recently been demonstrated by *Lee et al*. [2013] and by V. Pizzo et al. (Concepts for operational CME ensemble forecasting, submitted to *Space Weather*, 2015), the ambient solar wind background can significantly influence the CME arrival time and the results presented here corroborate those findings. Without using an ambient solar wind background that is representative of the observed conditions, we are unable to accurately predict the observed CME arrival time using realistic CME fit parameters. The ability to modify the ambient solar wind background input into WSA-Enlil in NRT could significantly reduce the errors in CME arrival times associated with cases when the background maps do not accurately reflect the current solar wind conditions through which the CME is propagated. Such corrections need to be applied in NRT any time a significant difference between the observed solar wind background and the model background becomes apparent. This is difficult to do since we do not definitively know the ambient solar wind background until the event reaches a solar wind monitoring satellite such as ACE; however, indications of a poor ambient may be observed 1–3 days ahead of the CME arrival allowing for corrections to be applied.

Another method that will likely improve the results is to continuously drive WSA-Enlil with updated photospheric magnetic field maps so as to produce a more realistic, time-evolving background solar wind. Given the current operational setup, only one photospheric field map is used to drive the WSA-Enlil model and the initial background does not evolve with time. However, if WSA-Enlil is driven with updated maps, this could potentially resolve some of the key issues concerning the proper description of the solar wind background discussed in this study.

In addition to correcting the model ambient solar wind background in NRT, the ability for space weather forecasters to modify the mass in the CME input is critical for accurately modeling large events such as

the 23 July 2012 event. As discussed in section 3, the mass of a CME input into the WSA-Enlil model is a function of the background solar wind density ρ, the CME half-width $\omega_{1/2}$, and the parameter dcld. A method to directly specify the CME mass may be more appropriate for massive CMEs, or at a minimum, running an ensemble where the parameter dcld is varied from the standard value of 4 to a larger value representative of a more massive CME. This would provide an estimate of the error associated with the uncertainty in the CME input mass.

This event study has also demonstrated the limitations given the current model setup to handle the case when an earlier CME alters the ambient background solar wind into which the second CME is cast. Such a problem could be addressed in two ways: First, as discussed above, the ambient model background could be modified in NRT to more closely match the observed ambient solar wind background. This method can be applied not only when a preceding CME results in preconditioned solar wind but anytime that a mismatch is observed between the current and model ambient background. The second method to account for the effects of a preceding CME would be to modify the way in which CMEs are configured in Enlil. Adjustments to the assumed shape of the CME as well as to the CME duration could allow for a localized low-density flow to form behind the first CME, mimicking the preconditioned solar wind through which the second CME transverses. A modified CME input shape could delay the time it takes the model to revert to the ambient background solar wind, possibly providing a more accurate description of the post-CME solar wind conditions. Such an alteration to the current operational setup could improve arrival time predictions any time multiple CMEs are observed in quick succession. As demonstrated in this case study, even a CME 4 days earlier can influence the propagation of a subsequent CME resulting in predicted arrival time errors of 10+ h, depending on the CME fit parameters and the ambient solar wind background.

In this paper, we have investigated the sensitivity of the unusually fast and strong 23 July 2012 CME to various model input parameters to understand how well we could forecast this type of event in NRT given the operational system currently employed by NOAA SWPC. We have quantified how variations in the initial CME speed, angular width, and direction, as well as the ambient solar wind background, affect the predicted arrival time of the CME at STEREO A, and we have discussed the factors involved in the fast transit time of this large CME. Three potential modifications to the operational version of the WSA-Enlil solar wind model have been presented which would enable improved forecasting of such an event had it been Earth directed. The large and impressive CME of 23 July 2012 would have produced a significant geomagnetic storm with potentially serious consequences had it impacted Earth instead of STEREO A, and thus, we must be able to accurately forecast the arrival times of such extreme events in NRT using realistic CME input parameters. Thus, improved NRT forecasting of future complex CME events may be achieved by correctly specifying the ambient solar wind background, incorporating methods to vary the CME input masses in an operational setup and integrating the effects of preconditioned solar wind due to any preceding CMEs.

Acknowledgments

This work was supported by the AFOSR Young Investigator Program grant FA9550-14-1-0262. SOHO coronagraph images were obtained from NASA's SOHO Science Archive (http://sohowww.nascom.nasa.gov). The STEREO A coronagraph images were obtained from NASA's STEREO Science Center Data Archive (http://stereo-ssc.nascom.nasa.gov), and the STEREO A solar wind plasma and magnetic field data were obtained from the PLASTIC Instrument Data Page (http://fiji.sr.unh.edu). Source surface synoptic charts were obtained from the Wilcox Solar Observatory website (http://wso.stanford.edu/synsourcel.html). This work utilizes data produced collaboratively between Air Force Research Laboratory (AFRL) and the National Solar Observatory (NSO). The ADAPT model development is supported by AFRL and Air Force Office of Scientific Research (AFOSR). The input data utilized by ADAPT are obtained by NSO/NISP (NSO Integrated Synoptic Program). NSO is operated by the Association of Universities for Research in Astronomy (AURA), Inc., under a cooperative agreement with the National Science Foundation (NSF). The GONG and ADAPT maps used in this study can be found at ftp://gong2.nso.edu/oQR/bqs and ftp://gong2.nso.edu/adapt/maps/special/Cash2015, respectively. The Enlil solar wind model used to run all CME simulations presented in this work is publicly accessible through the Community Coordinated Modeling Center at http://ccmc.gsfc.nasa.gov/models.

References

Altschuler, M. D., and G. Newkirk (1969), Magnetic fields and structure of solar corona. I: Methods of calculating coronal fields, *Solar Phys.*, *9*, 131–149.

Arge, C. N., and V. Pizzo (2000), Improvement in the prediction of solar wind conditions using near-real time solar magnetic field updates, *J. Geophys. Res.*, *105*, 10,465–10,479, doi:10.1029/1999JA000262.

Arge, C. N., D. Odstrcil, V. J. Pizzo, and L. R. Mayer (2003), Improved method for specifying solar wind speed near the Sun, in *Solar Wind Ten, Am. Inst. of Phys. Conf. Ser.*, vol. 679, edited by M. Velli et al., pp. 190–193, Am. Inst. of Phys., Melville, New York, doi:10.1063/1.1618574.

Arge, C. N., J. G. Luhmann, D. Odstrcil, C. J. Schrijver, and Y. Li (2004), Stream structure and coronal sources of the solar wind during the May 12th, 1997 CME, *J. Atmos. Sol. Terr. Phys.*, *66*, 1295–1309.

Arge, C. N., C. J. Henney, J. Koller, C. R. Compeau, S. Young, D. MacKenzie, A. Fay, and J. W. Harvey (2010), Air force data assimilative photospheric flux transport (ADAPT) model, in *Twelfth International Solar Wind Conference*, vol. 1216, edited by M. Maksimovic et al., pp. 343–346, AIP, Melville, New York.

Arge, C. N., C. J. Henney, J. Koller, W. A. Toussaint, J. W. Harvey, and S. Young (2011), Improving data drivers for coronal and solar wind models, in *5th International Conference of Numerical Modeling of Space Plasma Flows (ASTRONUM 2010)*, *ASP Conf. Ser.*, vol. 444, edited by N. V. Pogorelov, E. Audit, and G. P. Zank, p. 99, Astron. Soc. of the Pac., San Francisco, Calif.

Baker, D. N., X. Li, A. Pulkkinen, C. M. Ngwira, M. L. Mays, A. B. Galvin, and K. D. C. Simunac (2013), A major solar eruptive event in July 2012: Defining extreme space weather scenarios, *Space Weather*, *11*, 585–591, doi:10.1002/swe.20097.

Brueckner, G. E., et al. (1995), The large-angle spectroscopic coronagraph (LASCO), *Sol. Phys.*, *162*, 357–402.

Burkepile, J. T., A. J. Hundhausen, A. L. Stanger, O. C. St. Owy, and J. A. Seiden (2004), Role of projection effects on solar coronal mass ejection properties: 1. A study of CMEs associated with limb activity, *J. Geophys. Res.*, *109*, A03103, doi:10.1029/2003JA010149.

Colaninno, R. C., and A. Vourlidas (2009), First determination of the true mass of coronal mass ejections: A novel approach to using the two STEREO viewpoints, *Astrophys. J.*, *698*, 852–858, doi:10.1088/0004-637X/698/1/852.

Domingo, V., B. Fleck, and A. I. Poland (1995), The SOHO mission: An overview, *Solar Phys.*, *162*, 1–37.
Emmons, D., A. Acebal, A. Pulkkinen, A. Taktakishvili, P. MacNeice, and D. Odstrcil (2013), Ensemble forecasting of coronal mass ejections using the WSA-ENLIL with CONED Model, *Space Weather*, *11*, 95–106, doi:10.1002/swe.20019.
Harvey, J. W., et al. (1996), The Global Oscillation Network Group (GONG) project, *Science*, *272*, 1284–1286, doi:10.1126/science.272.5266.1284.
Henney, C. J., W. A. Toussaint, S. M. White, and C. N. Arge (2012), Forecasting $F_{10.7}$ with solar magnetic flux transport modeling, *Space Weather*, *10*, S02011, doi:10.1029/2011SW000748.
Hickmann, K. S., H. C. Godinez, C. J. Henney, and C. N. Arge (2015), Data Assimilation in the ADAPT photospheric flux transport model, *Sol. Phys.*, *290*, 1105–1118, doi:10.1007/s11207-015-0666-3.
Howard, R. A., et al. (2008), Sun Earth Connection Coronal and Heliospheric Investigation (SECCHI), *J. Space Sci. Rev.*, *136*, 67–115.
Kaiser, M. L., T. A. Kucera, J. M. Davila, O. C. S. Cyr, M. Guhathakurta, and E. Christian (2008), The STEREO Mission: An introduction, *Space Sci. Rev.*, *136*, 5–16, doi:10.1007/s11214-007-9277-0.
Lee, C. O., C. N. Arge, D. Odstrčil, G. Millward, V. Pizzo, J. M. Quinn, and C. J. Henney (2013), Ensemble modeling of CME propagation, *Solar Phys.*, *285*, 349–368, doi:10.1007/s11207-012-9980-1.
Liu, Y. D., et al. (2014), Observations of an extreme storm in interplanetary space caused by successive coronal mass ejections, *Nat. Commun.*, *5*, 3481, doi:10.1038/ncomms4481.
Mays, M. L., et al. (2015), Ensemble modeling of CMEs using the WSA-ENLIL + Cone model, *Sol. Phys.*, *290*, doi:10.1007/s11207-015-0692-1.
Millward, G., D. Biesecker, V. Pizzo, and C. A. de Koning (2013), An operational software tool for the analysis of coronagraph images: Determining CME parameters for input into the WSA-Enlil heliospheric model, *Space Weather*, *11*, 57–68, doi:10.1002/swe.20024.
Ngwira, C. M., A. Pulkkinen, M. Leila Mays, M. M. Kuznetsova, A. B. Galvin, K. Simunac, D. N. Baker, X. Li, Y. Zheng, and A. Glocer (2013), Simulation of the 23 July 2012 extreme space weather event: What if this extremely rare CME was Earth directed?, *Space Weather*, *11*, 671–679, doi:10.1002/2013SW000990.
Odstrcil, D. (2003), Modeling 3-D solar wind structure, *Adv. Space Res.*, *32*(4), 497–506.
Pizzo, V., G. Millward, A. Parsons, D. Biesecker, S. Hill, and D. Odstrcil (2011), Wang-Sheeley-Arge-Enlil cone model transitions to operations, *Space Weather*, *9*, S03004, doi:10.1029/2011SW000663.
Russell, C. T., et al. (2013), The very unusual interplanetary coronal mass ejection of 2012 July 23: A blast wave mediated by solar energetic particles, *Astrophys. J.*, *770*(38), doi:10.1088/0004-637X/770/1/38.
Schatten, K. H., J. M. Wilcox, and N. F. Ness (1969), A model of interplanetary and coronal magnetic fields, *Solar Phys.*, *6*, 442–455.
Temerin, M., and X. Li (2006), *Dst* model for 1995–2002, *J. Geophys. Res.*, *111*, A04221, doi:10.1029/2005JA011257.
Temmer, M., and N. V. Nitta (2015), Interplanetary propagation behavior of the fast coronal mass ejection from 23 July 2012, *Sol. Phys.*, *290*, 919–932.
Vršnak, B., et al. (2013), Propagation of interplanetary coronal mass ejections: The drag-based model, *Solar Phys.*, *285*, 295–315.
Wang, Y. M., and N. R. Sheeley Jr. (1992), On potential field models of the solar corona, *Astrophys. J.*, *392*, 310–319.